nature nanotechnology

SUPPLEMENTARY INFORMATION

DOI: 10.1038/NNANO.2012.217

Growth of a two dimensional dielectric monolayer on quasi-freestanding graphene

Rafik Addou, Arjun Dahal, Matthias Batzill

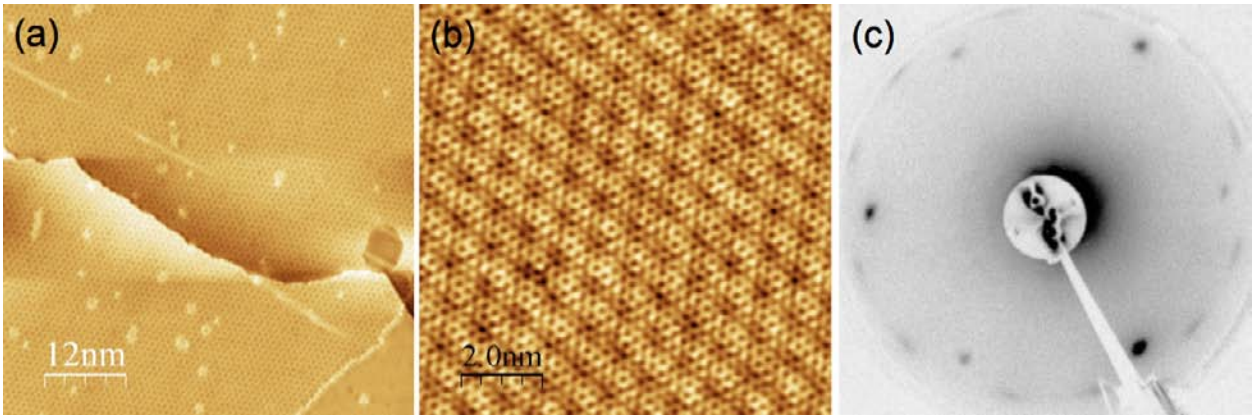

Fig. S1: STM and LEED study of graphene on Pt(111). Single layer graphene grown on Pt(111) forms various rotational domains that exhibit different moiré superstructures. In (a) an STM image one rotational domain covering most of the image and a second domain in the lower right corner is shown. The hexagonal structure that is visible in this large scale image is due to the moiré superstructure. (b) shows a higher resolution image which resolves the graphene honeycomb structure superimposed on a moiré structure. (c) shows the LEED pattern of graphene on Pt(111), taken with 60 eV electron energy.The LEED pattern of graphene on Pt(111) shows the Pt(111) 1×1 spots in addition to segments of a ring with a diameter corresponding to graphene. The ring segements indicate that many different rotational alignments relative to graphene are possible. The domain structures of graphene on Pt(111) has been thoroughly characterized previously, see e.g. ref. [1,2,3].(STM imaging conditions (a)V_{bias}= 150 mV I_t=1.8 nA; (b) V_{bias}= 5 mV I_t= 2 nA).

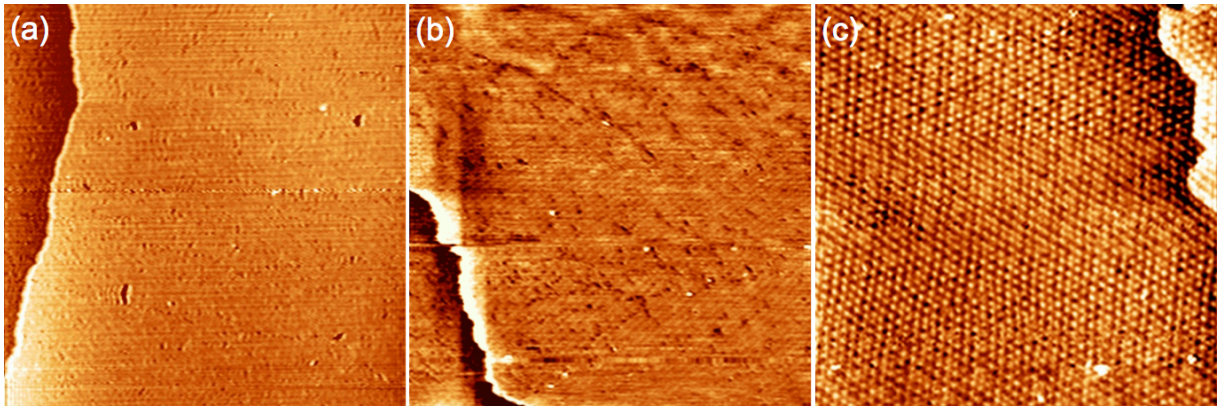

Fig. S2: STM images of annealing series of yttria/graphene/Pt(111). All images are 100 ×100 nm in size. (a) yttria film after room temperature deposition. No order can be discerned in STM but the film is very flat and no clustering is observed. (b) after annealing of the film to 400 °C. Still no order is observed (the faint ripple structure is due to instrumental noise) and (c) after annealing to 550 °C an ordered structure of the yttria film is observed.

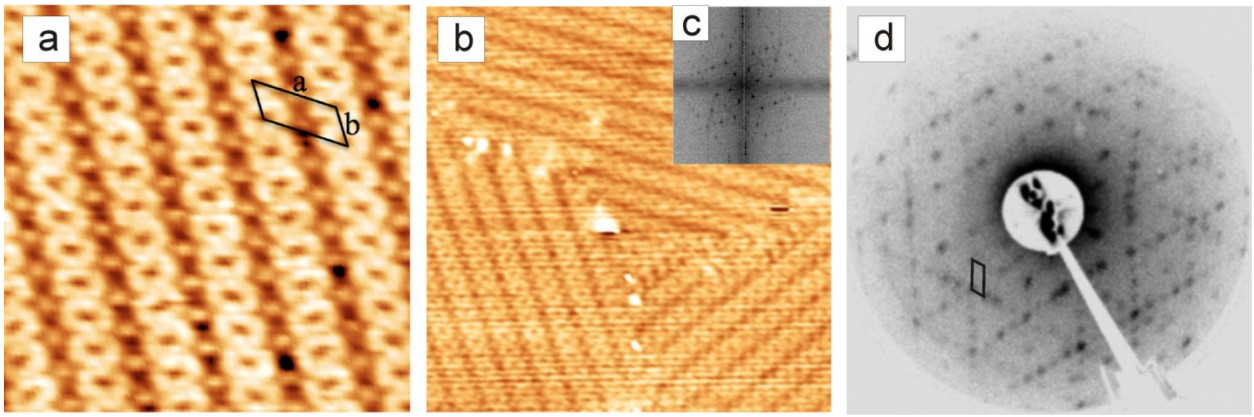

Fig. S3: STM and LEED study of yttria monolayer on pure Pt(111). (a) 10 nm x 10 nm STM image. The dimensions of the yttria unit cell as measured in the STM image are a= 0.97± 0.1 nm and b=2.32± 0.2 nm. This corresponds closely to a (2√3 × 5√3)R30° superstructure with respect to Pt(111), i.e. a = 0.96 nm and b = 2.40 nm. The existence of multiple domain structure as a consequence of the lower symmetry of the superstructure compared to the Pt(111) surface is shown in (b), where (c) is the Fourier transform of the STM image in (b). The LEED pattern of the superstructure is shown in (d) with the (2√3 × 5√3)R30° unit cell indicated. The electron energy for the LEED was 35 eV. In conclusion, STM and LEED indicates that a monolayer yttria forms a commensurate superstructure with respect to the Pt(111) substrate. (STM imaging conditions (a) V_{bias}= 2.5 V I_t= 0.1nA; (b) V_{bias}= 2 V I_t=0.3 nA).

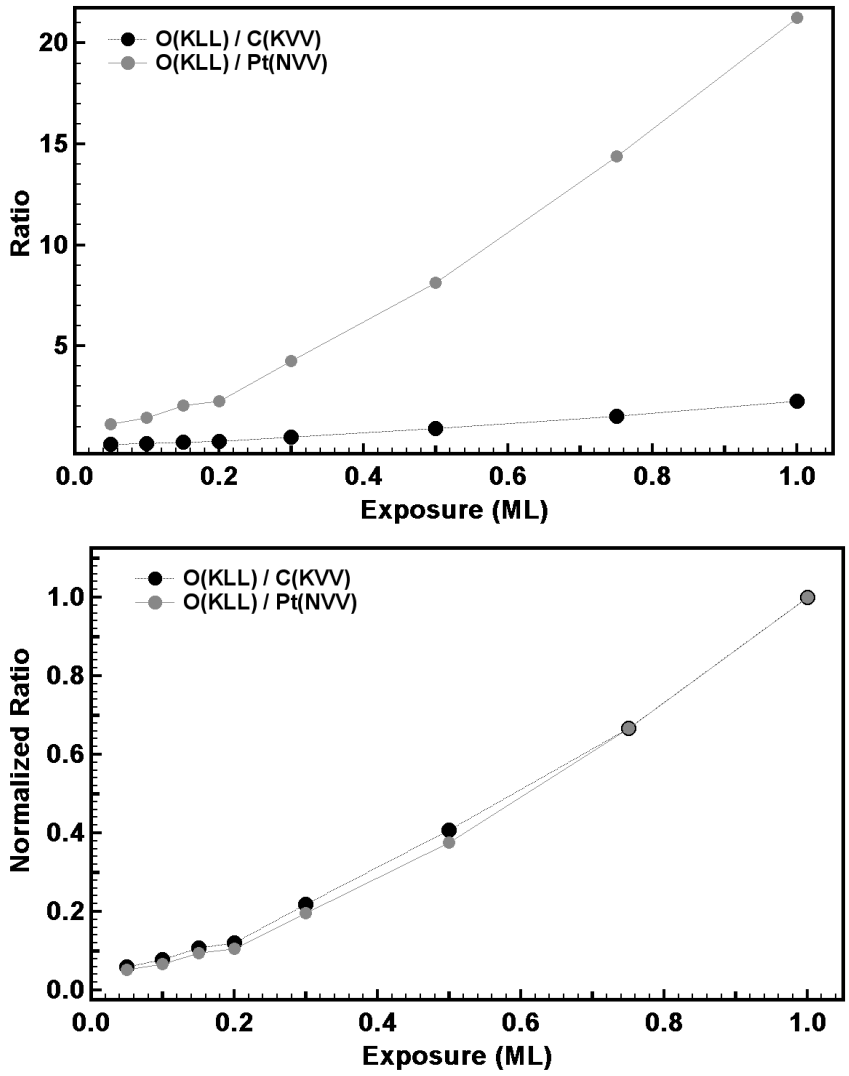

Fig. S4: Auger measurements for peak ratios of oxygen (yttrium oxide layer) to carbon (graphene) and oxygen to Pt(substrate) for increasing yttria growth and subsequent annealing to 600 °C. The top panel shows absolute ratios and the bottom panel after normalizing the two ratios. The fact that the two normalized ratios perfectly match each other indicates that a sandwich structure forms with yttria on top of the graphene/Pt(111) substrate and no intermixing occurs.

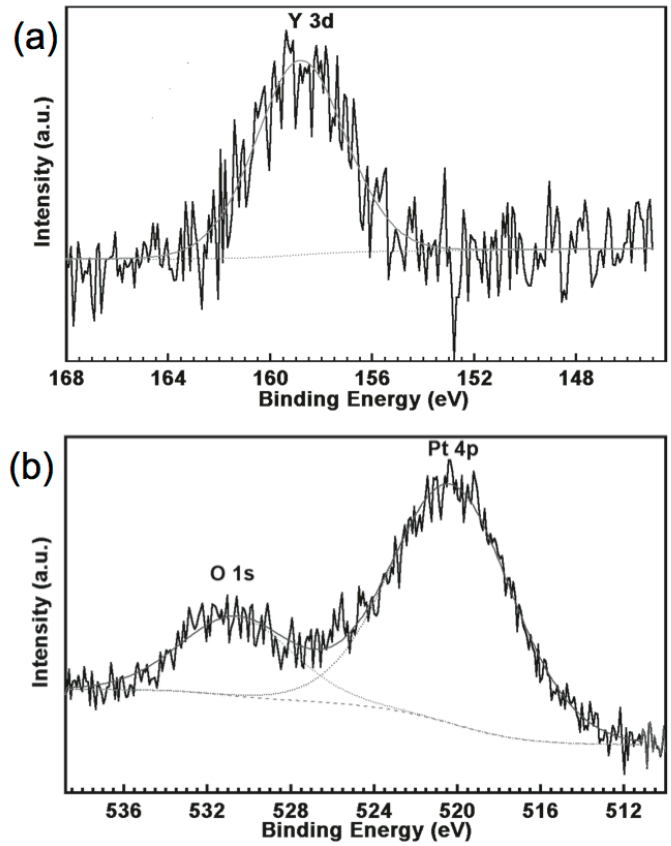

Fig. S5: XPS analysis of an yttria monolayer film grown on graphene/Pt(111) and annealed to ~600 °C. (a) Y-3d peak and (b) O-1s peak which is close to the Pt-4p peak.

Procedure for estimating O/C ratios in Auger measurements for a 2D oxide layer growth on graphene

Auger spectroscopy with its superior surface sensitivity is ideally suited for characterizing growth modes. In the case of yttria growth on graphene the oxygen to carbon peak intensities are measured, using the oxygen signal as a measure for the oxide. Taken the ratio of the two peaks ensures cancelation of any fluctuations in the instrumentation sensitivity between subsequent film depositions. In our experiments yttrium was evaporated in a 10^{-7} Torr oxygen atmosphere with the sample at room temperature. Subsequently the sample was annealed to a target temperature (550 °C for Ni, 600 °C for Pt and Ir) and then the AES spectra are taken. This procedure was repeated several times to build-up the monolayer. Figure 1(d) in the manuscript shows the O/C AES ratios for the different substrates, where we defined an O/C ratio of 2.2 as one monolayer of yttrium oxide. For a strictly two dimensional growth of an oxide layer on a single graphene layer the change in the ratio can be estimated by dividing the surface into (i) an oxygen covered surface (coverage Θ, with Θ=1 corresponding to a full monolayer) and (ii) a clean graphene surface. The oxygen intensity is a linear function of coverage Θ and scales with an AES oxygen sensitivity factor. The oxygen sensitivity factor is set to 2.4, a value reported in ref. [4] and measured for SiO_2 which has a similar O-density as Y_2O_3. The carbon intensity comes from two parts: (i) the uncovered fraction of the surface (1- Θ) and (ii) the fraction of the surface covered with the oxide (Θ). The total carbon intensity is the sum of these two contributions. For the uncovered fraction the carbon intensity is (1- Θ)×1.9, where the factor 1.9 is the estimated carbon sensitivity factor taken from ref. [4] measured on graphite. The carbon intensity on the covered fraction is being attenuated by the oxide layer by an attenuation factor of A= exp (-d/λ). In this expression d is the oxide layer thickness and λ the electron escape depth. Therefore the O/C ratio can be expressed as a function of oxide coverage Θ, as follows:

$$\frac{O}{C} = \frac{\Theta \times 2.4}{(1-\Theta)\times 1.9 + \Theta \times 1.9 \times A} \qquad (1)$$

To estimate the attenuation factor A, the electron escape depth λ was calculated using the equation given in ref. [5] as:

$$\lambda = E/[a(\ln E + b)] \qquad (2)$$

where E is the electron energy and a and b are Penn's coefficients which are equal to 18.3 and -2.95 respectively for carbon [5]. Thus for the carbon Auger electrons we obtain λ= 5.6 Å. The expected O/C ratio plotted in Fig 1(e) assumed an oxide layer thickness of d= 3 Å, which is a reasonable value for a monolayer thick oxide. Thus for these values of λ and d the attenuation factor is A=0.5856. Alternatively, we may use A as a fitting parameter to fit expression (1) to the measured data points. In this case we obtain A-values of 0.55, 0.54, and 0.57 for Pt, Ni, and Ir substrates, respectively. The very similar values for all three samples further indicate that the growth mode is the same, i.e. independent of the metal substrate.

Graphene charge doping and its determination by C-1s core level photoemission spectroscopy

An important observation in XPS is that the C-1s peak shifts by ~0.6 eV to higher binding energy upon adsorption of a monolayer of yttria on platinum supported graphene. As discussed, there is no indication for chemical bond formation between the yttria layer and graphene. Therefore the binding energy shift is unlikely to be a chemical shift. Instead we propose a universally applicable description of C-1s peak shifts of graphene with non-chemical interactions, i.e. systems with physisorbtion only. In this description a shift of the C-1s peaks is a consequence of Fermi-level shifts due to interface charge transfer doping. The correlation between core-level shifts in graphene and its Fermi-level position has not been previously demonstrated and thus we first establish the validity of such a model by carefully analyzing previously reported C-1s peak positions of metal supported graphene and comparing these shifts with expected (computed) Fermi-level shifts. The most comprehensive study of C-1s peak positions for graphene monolayers on different metals (Pt, Ir, Rh, Ru) was conducted by Preobrajenski et al.[6] For Pt and Ir, graphene only interacts weakly with the metal and only a single C-1s peak was found, while for Rh and Ru two C-1s peaks were detected in agreement with the notion of strongly and weakly interacting areas within a graphene moiré-superstructure unit cell. Here we only consider the weakly interacting areas that can be best described as physisorbed[7] graphene. In Fig. S6(a) we plot the C-1s peaks (physisorbed component) against the work function of the supporting metal, which clearly shows a correlation between the C-1s binding energy and the work function of the supporting metal. We explain this correlation by the fact that in XPS the binding energy is referenced to the Fermi-level and the Fermi-level in metal supported graphene may shift depending on interface charge transfer. This charge transfer, on the other hand, depends on the work function difference between the metal and graphene. In most hetero-layer systems the interface charge transfer does not result in a large Fermi-level shift. For graphene, the low density of states at the Dirac point, however, requires only a small charge transfer between the metal and graphene to cause measurable shifts. This shift of the Fermi-level in metal supported graphene has been experimental observed by angle resolved photoemission studies of the position of the Dirac point[8,9,10,11,12]. Metal induced charge transfer to graphene and the shift of the Fermi level has been computed for several metal substrates[13,14]. Using these computed Fermi-level values[13] we can estimate the C-1s core level position for different metal

substrates by subtracting the Fermi-level shift from the C-1s peak position of graphite (HOPG). Such estimated core-level positions are also plotted in Fig. S6(a) in order to compare it with the experimental values. The excellent agreement between estimated and measured C-1s peaks as a function of metal work function verifies our idea that the observed C-1s core level shift is predominantly a consequence of the shift of the Fermi-level in weakly interacting graphene heterosystems. Thus we conclude that in systems for which significant chemisorption can be excluded monitoring the C-1s peak by XPS during e.g. surface modification, is an easy and straightforward method for assessing changes in the charge doping of graphene.

For our studies, the analysis of C-1s peak shifts implies that the observed ~0.6 eV shift to higher binding energy is due to a shifting of the Fermi-level to above the Dirac point after yttria growth. Since Pt has one of the highest work functions of the transition metals (~ 5.7 eV)[15], the Fermi-level of Pt supported graphene is below the Dirac point (by ~0.3 -0.35 eV)[8,13] as illustrated in Fig. S6(b)[13,16]. The Fermi-level position can be shifted above the Dirac point by yttria growth, if the work function of the new surface layer consisting of a graphene/yttria composite is larger compared to that of graphene. Fig S6(c) illustrates such a scenario. A surface dipole of the yttria layer as would be the case in the atomic model shown in Fig 3(c) increases the surface work function, potentially to a higher value than that of Pt. This effectively reverses the doping of graphene from p-type on Pt to n-type for the Pt/graphene/yttria structure. Generally, these observations imply that we can significantly alter the charge transfer from metal contacts to graphene by a dipole layer on top of graphene. Such dipole layers could be ionic monolayers like demonstrated here or by adsorption of oriented molecules with a static dipole moment normal to the surface. It is important to point out, that in this concept it is not charge transfer from the adsorbate to graphene, as has been discussed previously[17], but rather it is the charge transferred from the metal substrate to graphene that causes the shift of the Fermi-level in graphene.

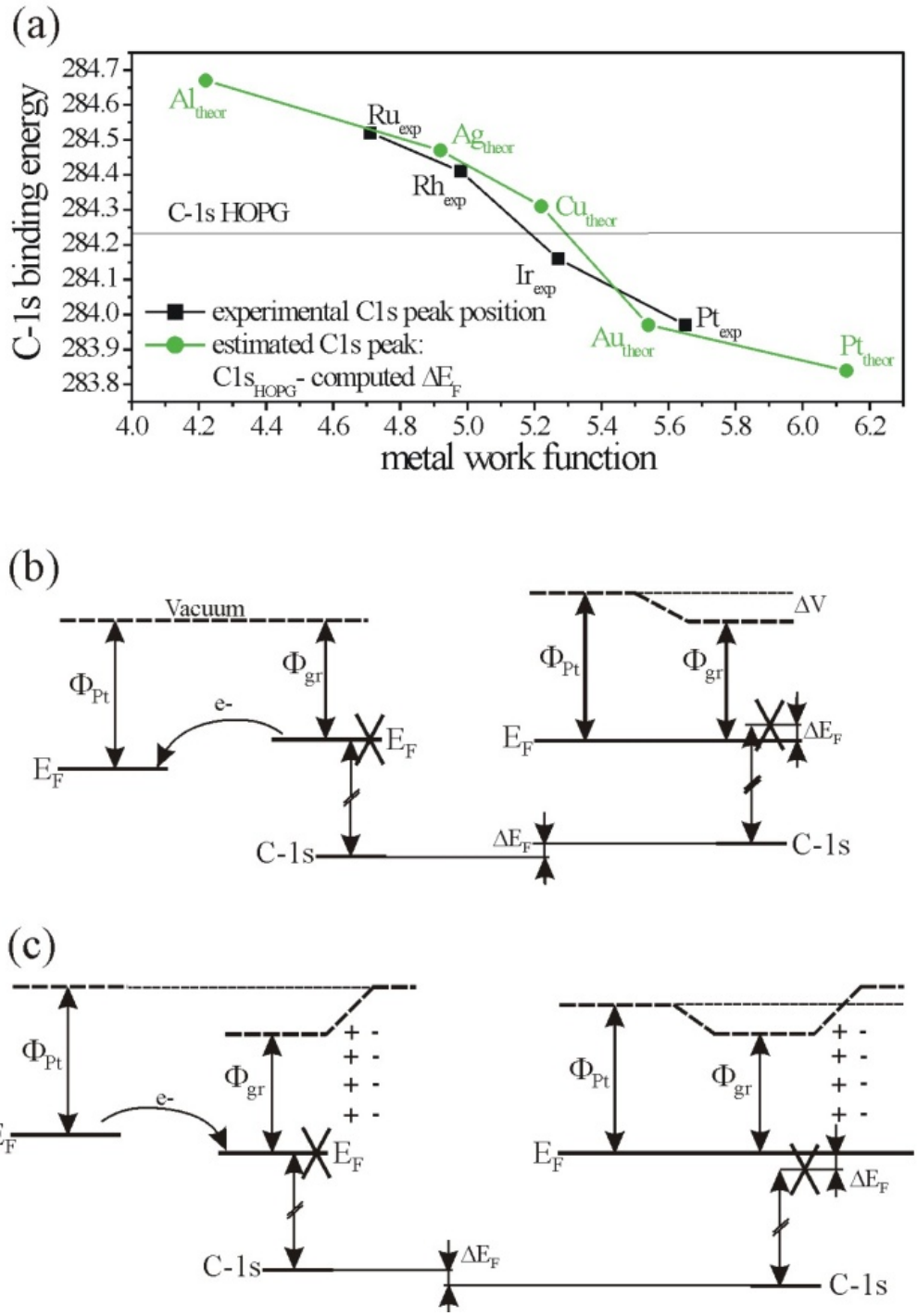

Figure S6: Explanation for graphene C-1s binding energy shift. In (a) experimentally observed C-1s peaks (taken from ref. [6]) or peak components due to weak interacting graphene are plotted versus the respective work function of the metal substrates (square data points). These data are compared to computed Fermi-level shifts (ΔE_F) for graphene interfaced with different metals (taken from ref. [13]). The C-1s peak is estimated by subtracting ΔE_F from the C-1s peak position of graphite (HOPG). The C-1s peak position estimated from computed ΔE_F is

then plotted as a function of the computed work function of the metal substrate. Note that for consistency experimental values for the work function are used in the experimental data and theoretical work function are used in the computed values. The agreement in the variation of the measured C-1s peak position with the computed Fermi-level shifts indicate that the C 1s peak can be used as a measure of the graphene Fermi-level as long as the graphene is only physisorbed on the metal. The relationship between C 1s, charge transfer due to work function differences, and the shift of the Fermi-level are illustrated in (b) for the case of graphene on Pt. The left side shows an energy-level diagram for Pt and graphene separated, and on the right after brought into contact. The effect of a static dipole layer (such as yttria) at the surface of graphene in illustrated in (c). The static dipole increases the work function of the graphene layer and thus if brought into contact with Pt, electrons are transferred from Pt to graphene shifting the Fermi-level above the Dirac point. Note the reversal of the C-1s peak shift in (c) compared to (b) relative to free-standing graphene.

Supplement references:

[1] P. Sutter, J.T. Sadowski, E. Sutter "Graphene on Pt(111): Growth and substrate interaction" Phys. Rev. B **80**, 245411 (2009).

[2] P. Merino, M. Svec, A.L. Pinnardi, G. Otero, J.A. Martin-Gago, "Strain-Driven Moire Superstructures of Epitaxial Graphene on Transition Metal Surfaces" ACS Nano **5**, 5627-5634 (2011).

[3] M. Gao, Y. Pan, L. Huang, H. Hu, L.Z. Zhang, H.M. Guo, S.X. Du, H.J. Gao," Epitaxial growth and structural property of graphene on Pt(111)" Appl. Phys. Lett. **98**, 033101 (2011).

[4] JEOL Handbook of Auger Electron Spectroscopy

[5] D.R. Penn, "Quantitative chemical analysis by ESCA" J. Electron Spectrosc. Related Phenomena, **9** (1976) 29

[6] A.B. Preobrajenski, M.L. Ng, A.S. Vinogradov, N. Mårtensson, Phys. Rev. B. **78**, 073401 (2008).

[7] T. Olsen, J. Yan, J.J. mortensen, K.S. Thygesen, Phys. Rev. Lett. **107**, 156401 (2011).

[8] P. Sutter, J.T. Sadowski, E. Sutter., Phys. Rev. B **80**, 245411 (2009).

[9] D. Marchenko, A. Varykhalov, A. Rybkin, A.M. Shikin, O. Rader, Appl. Phys. Lett. **98**, 122111 (2011).

[10] A.M. Shikin, V.K. Adamchuk, K.-H. Rieder, Phys. Solid State **51**, 2390-2400 (2009).

[11] I. Pletikosić, M. Kralj, P. Pervan, R. Brako, J. Coroaux, A.T. N'Diaye, C. Busse, T. Michely, Phys. Rev. Lett. **102**, 056808 (2009).

[12] E. Starodub, A. Bostwick, L. Moreschini, S. Nie, F. El Gabaly, K.F. McCarty, E. Rotenberg, Phys. Rev. B **83**, 125428 (2011).

[13] G. Giovannetti, P.A. Khomyakov, G. Brocks, V.M. Karpan, J. van den Brink, P.J. Kelly, Phys. Rev. Lett. **101**, 026803 (2008).

[14] C. Gong, D. Hinojos, W. Wang, N. Nijem, B. Shan, R.M. Wallace, K. Cho, Y.J. Chabal, ACS Nano **6**, 5381 (2012).

[15] H.L. Skriver, N.M. Rosengaard, Phys. Rev. B **46**, 7157 (1992).

[16] C. Gong, G. Lee, B. Shan, E.M. Vogel, R.M. Wallace, K. Cho, J. Appl. Phys. **108**, 123711 (2010).

[17] C. Coletti, C. Riedl, D. S. Lee, B. Krauss, L. Patthey, K. von Klitzing, J. H. Smet, U. Starke Phys. Rev. B **81**, 235401 (2010).